Appl. Chem. Eng., Vol. 33, No. 5, October 2022, 523-531
https://doi.org/10.14478/ace.2022.1082

Article

Influence of Urea Precursor on the Electrochemical Properties of Ni-Co-based Metal Organic Framework Electrodes for Supercapacitors

Ye Seul Jung, Yongju Jung* and Seok Kim†

School of Chemical Engineering, Pusan National University, Busan 46241, Korea
**Department of Applied Chemical Engineering, Korea University of Technology and Education, Cheonan 31253, Korea*
(Received July 21, 2022; Revised August 25, 2022; Accepted August 27, 2022)

Abstract

A NiCo-metal organic framework (MOF) electrode, prepared using urea as a surfactant, was synthesized using a one-pot hydrothermal method. The addition of urea to the NiCo-MOF creates interstitial voids and an ultra-thin nanostructure in the NiCo-MOF, which improves its charge transfer performance. We obtained the optimal metal to surfactant ratio to achieve the best specific capacitance. The NiCo-MOF was employed as the working electrode material in a three-electrode system. Field emission scanning electron microscopy, X-ray diffraction, and Fourier-transform infrared spectroscopy were employed to characterize the microstructures and morphologies of the composites. Cyclic voltammetry, galvanostatic charge-discharge, and electrochemical impedance spectroscopy curves were employed to quantify the electrochemical properties of the electrodes in a 6 M KOH electrolyte.

***Keywords**: Metal organic frameworks, Surfactant, NiCo-MOF, Electrochemical analysis, Supercapacitor*

1. Introduction

Owing to continuously increasing environmental challenges and volatility in the energy markets[1], many groups worldwide have focused on the development of novel energy storage systems. The development of renewable energy sources coupled with sustainable energy storage has become an important research topic[2,3]. Batteries and supercapacitors have received the most attention among the various mechanisms of energy storage[4]. Batteries offer a favorable energy density but possess a relatively low power density and are limited by their short lifecycle. In contrast, supercapacitors provide good power density but low energy density. Two main approaches have been developed to balance the power and energy density factors. The first is asymmetric cell design, which consists of a battery and capacitor electrode. A typical example would be Li-ion capacitors. The second approach is the development of electrodes that possess the dual characteristics of high power and energy density. A typical example is a two-component electrode-based supercapacitor[5,6]. There are two types of supercapacitors: electric double-layer capacitors (EDLCs) and pseudocapacitors. EDLCs utilize activated carbon, graphene, and carbon nanotubes (CNTs), which are porous carbon materials with high surface areas that accumulate charges at the electrode/electrolyte interface based on an electric double layer mechanism. Conversely, pseudocapacitors store electric charges through a rapid, reversible redox reaction between the electrode and electrolyte; the constituent materials are primarily metal compounds and polymer ion gel electrolytes[7,8]. Pseudocapacitors are capable of much higher charge storage than EDLCs owing to near-surface redox reactions[8].

Metal organic frameworks (MOFs) with high surface areas and excellent pore sizes are among the most suitable electrode materials for supercapacitors[9,10]. They are used as active materials or sacrificial templates for supercapacitors because their highly porous metal organic cages provide sufficient redox sites and enhance ion diffusion[11]. MOFs are porous materials consisting of three-dimensional structures based on coordination with organic ligands around metal clusters[12]. Compared with other nanomaterials, MOFs possess a large specific surface area, while their constituent elements can be easily tuned to design pores with specific physical, chemical, and electrical functionality[13].

By synthesizing electrodes using an MOF, we can compensate for the shortcomings of slurries by growing the material directly on the electrode. For example, in the case of powdery materials, a conductive agent and a polymer binder are required to manufacture the supercapacitor electrode. This increases the contact resistance of the electrode; however, it also lowers its overall energy storage capacity and performance given that the active site is buried and mass transport is suppressed[14]. In addition, these nanomaterials in powder form can easily peel off from the substrate during long-term measurements, resulting in poor durability. Hence, the electrode in powder form may possess limited applicability in terms of improving the electrochemical performance[15].

The use of organic binders in electrode fabrication can result in burial of active sites and suppression of mass transport, which may under-

† Corresponding Author: Pusan National University
School of Chemical Engineering, Busan 46241, Korea
Tel: +82-51-510-3874 e-mail: seokkim@pusan.ac.kr

pISSN: 1225-0112 eISSN: 2288-4505

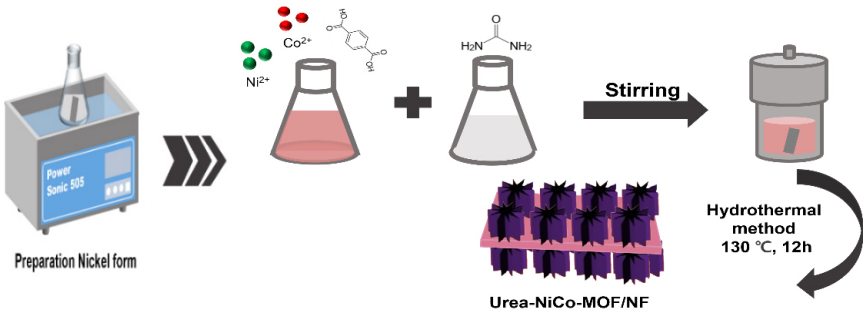

Figure 1. Process for preparation of MOF-based composite electrode[31,32].

mine electrochemical performance enhancements. In addition, the limited contact area between the nanostructure material and the substrate can lead to low mass loading and high contact resistance[10].

Therefore, a more effective method is to form binder-free electrodes with a 3D interconnected network of materials by growing them directly on a conductive substrate; this will efficiently transport electrons and ions during redox reactions[16,17]. Nickel foam (NF), as a conductive substrate, possesses a desirable 3D macroporous structure, high specific surface area, and favorable physical strength, making it a promising substrate for MOF-based supercapacitors[18].

In situ growth is characterized by the following advantages: First, no organic binders or conductive agents are required, which greatly simplifies the preparation process. Second, in situ growth in a vertical arrangement can uniformly disperse the active nanomaterials, providing sufficient surface area for electrochemical reactions. Third, the vertical arrangement in which the active material and the conductive substrate are in close contact provides a short ion diffusion path while ensuring low contact resistance and high electron conduction. Therefore, these advantages are advantageous for improving the electrochemical properties of vertical standing arrays for supercapacitors due to direct growth on the substrate[15].

In supercapacitors, the electrode material is the key component determining the electrochemical performance and safety of the fabricated device. Various transition metals such as Ni, Co, Mn, and Ru have been proposed as high energy density materials for supercapacitor applications given their high capacity, excellent electrical conductivity, and robust properties[19]. Bimetals possess a high energy power density, support surface reversible redox reactions, and are relatively safe, making them favored candidates for supercapacitor applications[20,21]. In particular, nickel materials possess a very high theoretical capacity, though there is a need to improve their cycle safety. Nickel cobalt bimetal has received considerable attention as an electrode material for energy storage applications owing to its promotion of synergistic effects[21]. As bimetal electrodes, Ni and Co are adjacent elements in the periodic table and possess comparable atomic radical and chemical valence states. The components of the resulting material can be synthesized by controlling the initial ratio of Ni^{2+} to Co^{2+} ions[22,23].

In this study, we report the synthesis of a vertical-standing array nickel–cobalt-based MOF by introducing urea as a surfactant to modify the nanostructure. Surfactants possess many unique solvent properties, such as negligible vapor pressure, high thermal stability, and increased solubility of the metal ions and organic ligands[24]. They also play a vital role in the efficient control of the size and shape of the targeted MOF nanocrystals[25].

Based on the aforementioned analysis, a bimetallic MOF was synthesized via a hydrothermal route through the determination of the optimal Ni to Co ratio. To improve the electrochemical performance, urea was introduced to the NiCo-MOF electrode material. According to the scanning electron microscopy (SEM), X-ray diffraction (XRD), and Fourier-transform infrared spectroscopy (FT-IR) analyses, the morphological shape and structure of the material varied as a function of the urea concentration.

The obtained material was directly grown on nickel foam by an in situ synthesis method and utilized as a binder-free electrode. The synergistic effect of Ni and Co combined with the addition of urea facilitated a distinct capacitive redox reaction and a high specific capacity of 838 F/g at 2 A/g. The developed material was demonstrated as being a suitable electrode for capacitors as it improved their electrochemical performance.

2. Experimental section

2.1. Materials

Nickel nitrate hexahydrate ($Ni(NO_3)_2 \cdot 6H_2O$, ≥97.0%, Daejung), cobalt nitrate hexahydrate [$Co(NO_3)_2 \cdot 6H_2O$, ≥98.0%, Sigma-Aldrich], terephthalic acid ($C_8H_6O_4$, ≥97.0%, Daejung), and urea (NH_2CONH_2, ≥99.0%, Yakuri Pure Chemicals) were used as received without further purification. N,N-dimethylformamide (DMF, ≥99.8%) was purchased from Alfa Aesar, and hydrochloric acid (HCl, ≥35%, Daejung) was used without further purification. Anhydrous ethyl alcohol (C_2H_5OH, ≥99.9%, Daejung) and potassium hydroxide (KOH, ≥85%, Sigma-Aldrich) were used as received without further purification.

2.2. Synthesis of NiCo-MOF

Consistent with the standard procedure, a fragment of Ni foam (2 × 5 cm) was cleaned and etched with 6M HCl for 5 min to remove the oxide layer on the surface. It was then washed by successive sonication with deionized water and absolute ethanol for several minutes, and subsequently dried in a vacuum for standby application.

NiCo-MOF composites were synthesized via a simple hydrothermal

route. For example, using a 1:1 ratio of nickel to cobalt, 0.62 mmol of $Ni(NO_3)_2.6(H_2O)$, 0.62 mmol of $Co(NO_3)_2.6(H_2O)$, and 1.265 mmol of terephthalic acid were mixed in 50 mL DMF under vigorous magnetic stirring for 15 min and transferred to a 120 mL Teflon-lined stainless-steel autoclave containing the cleaned nickel foam sheet.

The autoclave was then sealed and heated to 130°C for 10 h. After cooling to room temperature, the samples were washed under sonication in DMF, ethanol, and distilled water and dried at 50 °C for 8 h.

Various nickel-to-cobalt ratios (1:1, 1:2, 2:1, 2:3) were prepared by varying the amounts of nickel and cobalt salts, maintaining the total concentration of all transition metal salts at 1.24 mmol.

2.3. Synthesis of Urea-NiCo-MOF composite

The urea-NiCo-MOF composites were also synthesized via a simple hydrothermal route. 0.41 mmol of $Ni(NO_3)_2.6(H_2O)$, 0.83 mmol of $Co(NO_3)_2.6(H_2O)$ and 1.265 mmol of terephthalic acid were combined in 40 ml of DMF under vigorous magnetic stirring for 10 min. Various amounts (1 mmol, 2 mmol, 4 mmol, 8 mmol) of urea were added to 10 ml distilled water and stirred for 5 min.

The sample nomenclature corresponded to the amount of urea: 1U-NiCo-MOF (urea 1 mmol); 2U-NiCo-MOF (urea 2 mmol); 4U-NiCo-MOF (urea 4 mmol); 8U-NiCo-MOF (urea 8 mmol). The two solutions were mixed, and the mixture was vigorously stirred for 15 min. The reaction conditions of U-NiCo-MOF were the same as those of NiCo-MOF.

2.4. Electrochemical measurement

The NiCo-MOF and urea-NiCo-MOF electrodes were grown on (in situ) nickel foam (1 × 1 cm) as a current collector. A saturated calomel electrode (SCE) and a Pt wire were used as the reference and counter electrodes, respectively. The measurements were performed in 6 M aqueous KOH electrolyte. Cyclic voltammograms (CV) were acquired at −0.3 to 0.6 V at different scan rates. Galvanostatic charge-discharge (GCD) curves were obtained in the potential range of 0 to 0.45 V at various current densities. The electrochemical impedance spectroscopy (EIS) of the material was performed in the frequency range of 0.1 Hz to 100 kHz.

2.5. Characterization

To investigate the microstructure of the composite, X-ray diffraction (XRD, X-Ray Diffractometer(XRD) XRD-Xpert3) patterns were acquired with Cu-Kα radiation in the 2θ range 5~80°, whereas Fourier-transform infrared (FT-IR, Perkin Elmer Spectrum GX) spectroscopic analysis was performed in the wavelength range 600~4000 cm^{-1}. We also analyzed the morphology and microstructure of the composites via field-emission scanning electron microscopy (FE-SEM, SUPRA25) and energy-dispersive X-ray spectroscopy (EDS, X-max 80 mm^2).

3. Results and discussion

3.1. Materials characterization

In Figure 2(1), FT-IR spectra were obtained to confirm the specific

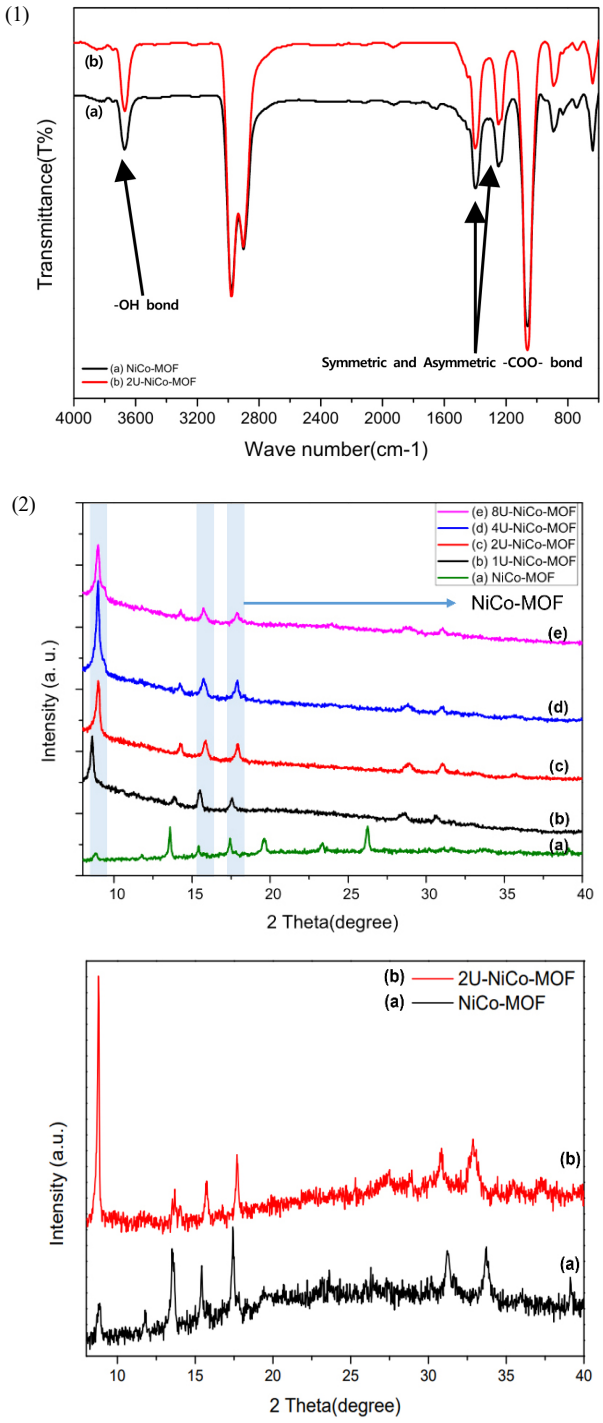

Figure 2. (1) FT-IR spectra of (a) NiCo-MOF; (b) 2U-NiCo-MOF (2) XRD patterns of (a) NiCo-MOF, (b) 1U-NiCo-MOF, (c) 2U-NiCo-MOF, (d) 4U-NiCo-MOF, and (e) 8U-NiCo-MOF.

chemical bond of the NiCo and U-NiCo MOFs. Peaks at 1404 and 1250 cm^{-1} in two vibrational bonds were identified for each material and assigned to the symmetric and asymmetric vibrations of the carboxyl bond, respectively[24]. This absorption bond differs from that of the C=O straight bond given that the weak C=O breaks from the carboxyl group of terephthalic acid to form the COO−Co frameworks.

Broad bonds (3600~3000 cm^{-1}) contribute to the OH linear vibration, which forms hydrogen bonds in the structure[26].

Therefore, the bonding of Ni,Co metals and terephthalic acid (ligand) organics to form NiCo-MOF was confirmed as three representative distinct peaks at 1500 and 1300 cm^{-1} and 3600–3000 cm^{-1}. The IR peak of NiCo-MOF with urea and that of NiCo-MOF without urea were identical. So, urea only acts as a surfactant and does not affect bonding[31].

From Figure 2(2), the peak value at 2θ indicates a nickel-cobalt-based MOF or a Petal-like layered MOF to which U-NiCo-MOF are assigned[27,28].

NiCo-MOF exhibits three main peaks at 8.8°, 16°, and 18.2°, which are indexed to the (200), (001), and (201) planes, respectively; they are characteristic of ultrathin NiCo-MOF nanosheets synthesized with BDC ligands[29,30]

The addition of urea to the NiCo-MOF synthesis process resulted in a relatively low peak at 8.9°; the peak intensity of U-NiCo-MOF at a 2θ value of 8.9° was relatively high compared to other NiCo-MOF peaks[31,32].

The XRD peak of NiCo-MOF with urea and that of NiC-MOF without urea were identical. Therefore, it is inferred that urea will not affect the structure when bound to MOFs. These peaks are in good agreement with those of previously reported literature studies[32]. These results demonstrate that the addition of urea was successfully synthesized along the surface of MOFs without damaging the crystal structure of NiCo-MOF.

SEM images of the NiCo-MOF materials with different nickel and cobalt metal concentrations are shown in Figure 3.

The thickness of the MOF for each ratio is as follows: (a) 31 nm; (b) 26 nm; (c) 33 nm; (d) 36 nm. Fine NiCo-MOF crystals of less than 2 μm were shown as possessing a petal-like appearance. Following the hydrothermal synthesis reaction, a NiCo-MOF with a relatively smooth surface was formed. In the case of this ratio, this difference in shape is reflected in the electrochemical performance of the corresponding electrode. It can be seen in Figure 3 (a) that vertical-standing arrays of MOF nanostructures were generated at the Ni:Co = 1:1 ratio. As shown in the SEM image of Ni:Co = 1:2 [Figure 3(b)], it was confirmed that this ratio is the optimal ratio given that its electrochemical performance is increased due to its thin and porous structure. Their highly open structures offer all the advantages of nanostructures, reducing the ion diffusion length while providing a high specific surface area available for charge storage[8,9]. In the case of Ni:Co = 2:1 [Figure 3(c)], there is agglomeration to form an elliptical structure. In this case, the redox reaction is ineffective; the capacitor performance is also deteriorated. As shown in the SEM image of Ni:Co = 2:3 [Figure 3(d)], its thickness is more than that of the structures shown in Figure 3(a) and (b), while its surface is uneven. As can be seen in the figure, if the thickness is increased, the specific surface area and resulting electrochemical performance are also reduced. Therefore the optimal bimetal ratio exhibiting the most favorable performance of the NiCo-MOF is the Ni:Co ratio, 1:2.

As a result of the addition of urea, NiCo-MOF crystals grew effectively on the Ni foam and exhibited regular shapes, indicating that they were firmly fixed on the surface of the Ni foam. It can be seen that U-NiCo-MOFs also grew effectively on Ni-form surfaces, characterized by a petal-like crystal structure. The addition of urea improved the electrochemical conductivity of pseudocapacitors over that of NiCo-MOF materials.

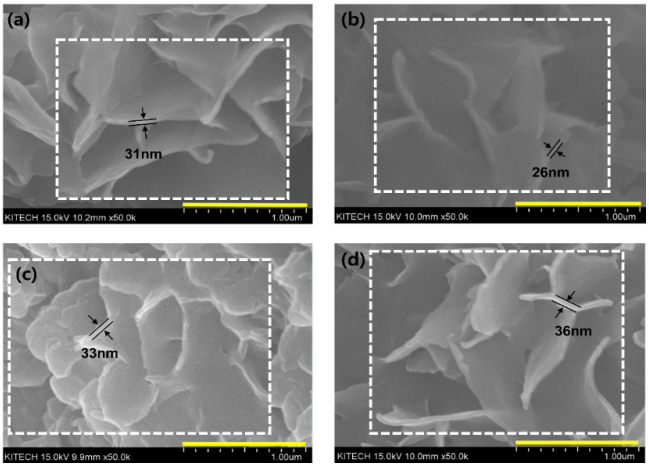

Figure 3. SEM of NiCo-MOF (a) Ni:Co = 1:1; (b) Ni:Co = 1:2; (c) Ni:Co = 2:1; (d) Ni:Co = 2:3.

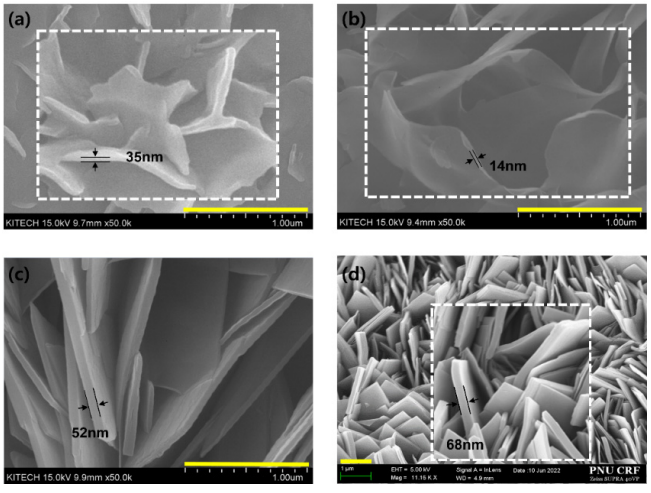

Figure 4. SEM of (a) 1U-NiCo-MOF; (b) 2U-NiCo-MOF; (c) 4U-NiCo-MOF; (d) 8U-NiCo-MOF.

Figure 4 presents the SEM image of the MOF for each urea concentration. The thickness of the urea-NiCo-MOF for each ratio is as follows: (a) 35 nm; (b) 14 nm; (c) 52 nm; (d) 68 nm

SEM analysis of fabricated U-NiCo-MOFs (Figure 4) demonstrated that the electrodes possessed a three-dimensional structure, exhibiting a nano-scale thickness with petal-like appearance through the addition urea in various proportions. The nanoflakes were generated along with vertical-standing arrays at a low concentration of 1.0 mmol urea (1U). The growth of these nanoflakes continued with increased urea concentrations up to 2.0 mmol urea (2U)[Figure 4(b)] In the case of 2U, as shown in the SEM image, the MOF is thinner and possesses a more porous structure than the case of MOF with 1.0 mmol urea. This in-

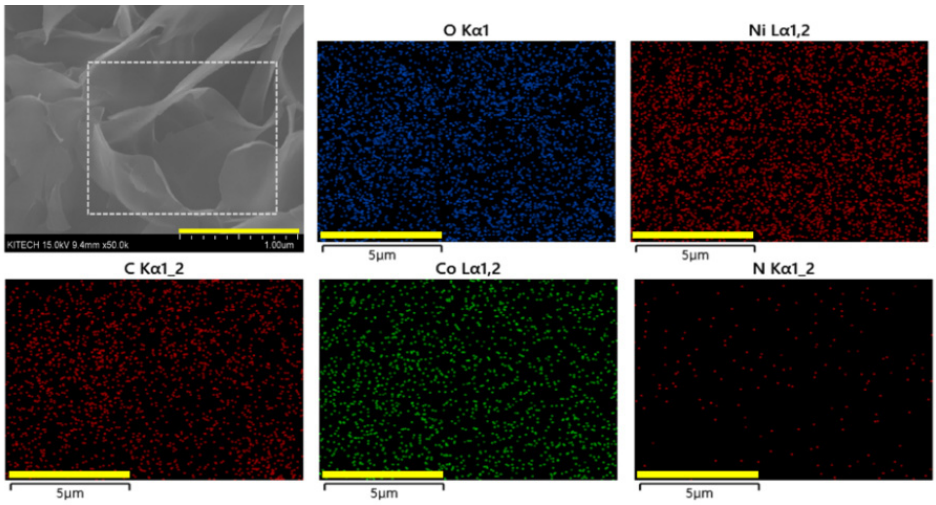

Figure 5. EDS elemental mapping images of Urea-NiCo-MOF: 2U-NiCo-MOF section.

dicates that the production of ammonium hydroxide at this urea concentration plays an important role in the morphogenesis and growth of urea-NiCo-MOF nanostructures[19] As the concentration of urea increases to 4.0 mmol urea (4U), as shown in the corresponding SEM image[Figure 4(c)], the synthesized material develops a thick plate shape; however, slight cracks form on the surface. When the urea concentration is further increased up to 8.0 mmol urea (8U)[Figure 4(d)], the overall nanostructure becomes thick and entangled due to overgrowth.

This petal-like nanostructure of urea-NiCo-MOF provides a more active surface area for effective intercalation of electrolyte ions useful for SC applications. Urea provides a slow supply of hydroxide ions upon gradual hydrolysis, which is key to controlling the precipitation of bimetallic hydroxides and regulating their anisotropic growth[33]. Cobalt also serves to stabilize the anisotropic growth and final formation of three-dimensional nanostructures, as it results in the formation of nanosheets rather than nanowires, consistent with previous reports[34,35]. When both cobalt and nickel are present in the solution, competition occurs between carbonate and hydroxide ions in their respective nickel-to-cobalt ratios to react with nickel and cobalt ions, which affects the morphology, crystallinity, and topology of the precipitate[35].

EDS element mapping is also performed to identify the distribution of specific elements (Figure 5). The U-NiCo-MOF section mainly comprises Ni, Co, O, N, and C, which can be attributed to the urea-NiCo-MOF with a diffused Ni^{+} ion obtained from the Ni foam during the hydrothermal reaction.

3.2. Electrochemical characterization

NiCo-MOF samples with various metal ratios were evaluated using a three-electrode system and CV curves were obtained at a scan rate of 30 mV s-1 in a potential range of -0.3 to 0.6 V in 6M KOH electrolyte. All the samples exhibited clear redox peaks owing to their pseudocapacitive properties.

When the CV curves were compared [Figure 6(1)], the NiCo-MOF 1:2 electrode was the largest compared to the other NiCo-MOF cases (1:1, 2:1, and 2:3 ratios). Therefore, after setting the metal ratio as Ni:Co = 1:2, the urea concentration was varied to isolate its impact on electrode performance.

The sample nomenclature corresponded to the amount of urea: 1U-NiCo-MOF (urea 1 mmol); 2U-NiCo-MOF (urea 2 mmol); 4U-NiCo-MOF (urea 4 mmol); 8U-NiCo-MOF (urea 8 mmol). The urea content corresponding to the 2U case [Figure 6(2)] exhibited the largest surface area and strongest redox peak. The 2U-NiCo-MOF sample exhibited very strong oxidation and reduction peaks at 0.5 V and 0.06 V, respectively; the variations in redox peaks can be determined for each sample. This result can be understood in terms of the fact that the 2U sample possesses more reactive sites owing to its larger specific surface area and better electrical conductivity[36]. The electrode material U-NiCo-MOF, with a three-dimensional layer structure, can provide sufficient space for the intercalation and deintercalation of OH^{-}[37].

The U-NiCo-MOF porous microstructure obtained by synthesizing NiCo-MOF provides a high specific capacitance by promoting high-speed charge transfer on the template and exposure of active sites to the electrolyte.

The GCD test was also performed at a potential of 0−0.45V; the samples exhibited typical pseudocapacitance behavior at various current densities ranging from 1 to 7 A/g.

Figure 6(3) shows the GCD graph of the NiCo-MOF samples of various ratios and demonstrates trends comparable to those of the CV results. NiCo MOF 1:2 possesses the longest discharge time and favorable capacitive properties. The length of discharge time decreases in the order of Ni:Co = 1:2, 1:1, 2:3, and 2:1. The specific capacitance (Cs) of the samples was calculated using the equation: Cs = I t /m V, where I is the discharge current (A), t is discharge time (s), m is the mass of the working electrode (g) and V is the potenial range of discharge (V)[38]. The capacitances of NiCo-MOF 1:2, 1:1, 2:3, and 2:1 are 520, 366, 270, and 260 F/g, respectively, at a current density of 2 A/g.

Compared with the other samples, it was confirmed that the redox

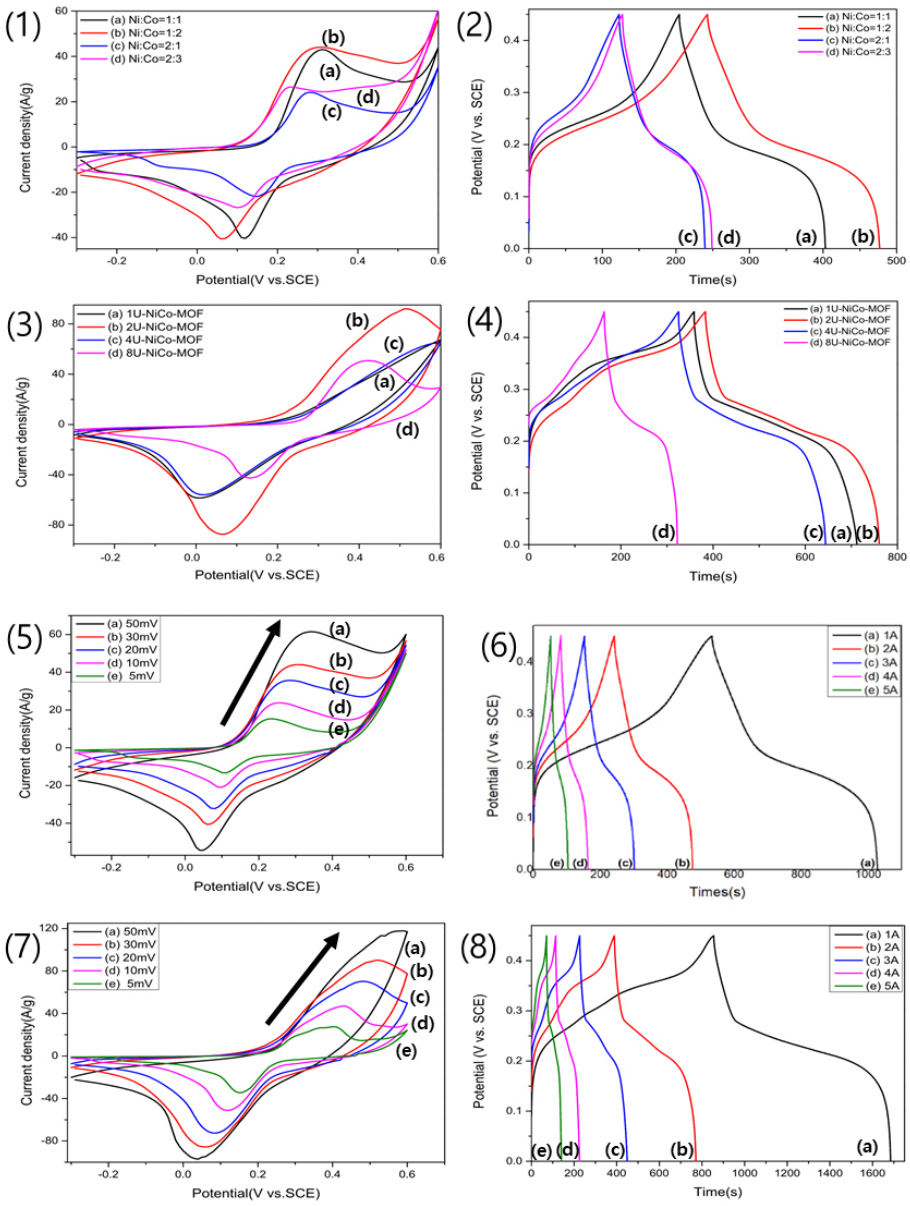

Figure 6. (1) CV curves of the (a) Ni:Co = 1:1, (b) Ni:Co = 1:2, (c) Ni:Co = 2:1, and (d) Ni:Co = 2:3 cases at a scan rate 30 mV/s (2) CV curves of the (a) 1U, (b) 2U, (c) 4U, and (d) 8U at a scan rate 30 mV/s (3) GCD curves of the (a) Ni:Co = 1:1, (b) Ni:Co = 1:2, (c) Ni:Co = 2:1, and (d) Ni:Co = 2:3 at a current density of 2 A/g (4) GCD curves of the (a) 1U, (b) 2U, (c) 4U, and (d) 8U at a current density of 2 A/g (5) CV curves of NiCo-MOF at the scan rates of (a) 5, (b) 10, (c) 20, (d) 30, and (e) 50 mV/s (6) CV curves of U-NiCo-MOF at the scan rates of (a) 5, (b) 10, (c) 20, (d) 30, and (e) 50 mV/s (7) GCD curves of NiCo-MOF at the current densities of (a) 1, (b) 2, (c) 3, (d) 4, and (e) 5 A/g (8) GCD curves of 2U-NiCo-MOF at the current densities of (a) 1, (b) 2, (c) 3, (d) 4, and (e) 5 A/g.

peak was reduced in the case of 8U-NiCo-MOF, which possessed the highest urea content. The addition of excess urea to M-MOF increased nanoparticle aggregation. The response area of the 8U-NiCo-MOF electrode was expected to decrease compared to that of the 2U-NiCo-MOF electrode.

The GCD curve of 2U-NiCo-MOF is also shown in Figure 6(4). 1U-NiCo-MOF, 2U-NiCo-MOF, 4U-NiCo-MOF, and 8U-NiCo-MOF produced specific capacitances of 785, 838, 708, and 352 F/g respectively, at a current density of 2 A/g. Therefore, the highest capacitance was achieved with 2U-NiCo-MOF.

In this study, the capacitive behavior of the composite electrode was attributed to the synergistic effect of urea and M-MOF. The 2U-NiCo-MOF electrode exhibited the most favorable charge–discharge duration and excellent capacitance. A decrease in device performance was observed when the amount of urea was increased by a factor of four with respect to the amount of urea.

To demonstrate the effect of scan rate, various scan rates such as 5, 10, 20, 30, 50 mV/s were applied to the NiCo-MOF and

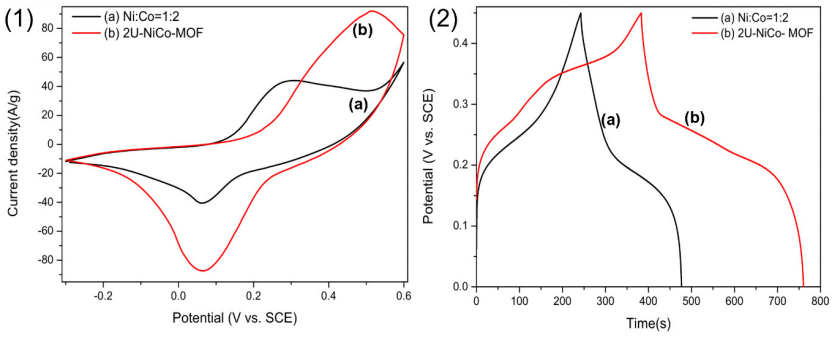

Figure 7. (1) CV curves of the (a) NiCo-MOF and (b) 2U-NiCo-MOF at a scan rate 30 mV/s (2) GCD curves of the (a) NiCo-MOF and (b) 2U-NiCo-MOF at a current density of 2 A/g.

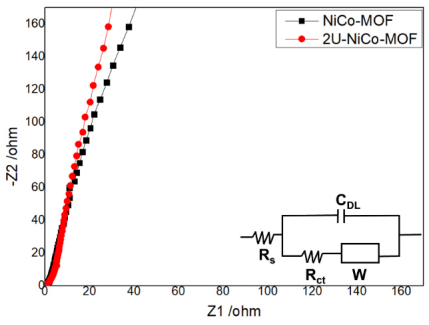

Figure 8. Nyquist plot of the NiCo-MOF and 2U-NiCo-MOF.

2U-NiCo-MOF samples [Figure 6(5), (6)]. The non-rectangular shape is maintained at all scan rates to exhibit a capacitive behavior comparable with that of nanosheets, facilitating rapid redox reactions and ion diffusion into porous surfaces[39].

CV and GCD plots were obtained to compare the electrochemical performance of the Ni-Co-MOF and the 2U-NiCo MOF electrodes [Figure 7(1) and (2)]. Comparison of the CV curves of the NiCo-MOF electrode and 2U-NiCo-MOF at a scan rate of 30 mV/s confirmed that the 2U-NiCo-MOF exhibited a stronger redox peak for Ni-Co than the NiCo-MOF electrode. GCD tests were performed in a potential window of 0~0.45 V (relative to the SCE reference electrode) at a current density of 2 A/g. The discharge time of 2U-NiCo-MOF was longer than NiCo-MOF, consistent with the calculated specific capacitances of 520 and 838 F/g, respectively, at current densities of 2 A/g. Therefore, the U-NiCo-MOF electrode demonstrated excellent electrochemical properties through the addition of urea to NiCo-MOF.

Electrochemical impedance spectroscopy (EIS) data were acquired over a frequency range of 0.1 Hz to 100 kHz and the corresponding Nyquist plots are shown in Figure 8. The measured impedance data is analyzed with electrical factors such as electrolyte resistance (Rs), charge transfer impedance (Rct), Warburg impedance (W), and phase factor (CPE). The plot slopes in the low frequency range differed, suggesting that the ion diffusion behavior was improved for 2U-NiCo-MOF due to the high porosity of NiCo-MOF.

4. Conclusions

In this study, we synthesized a metal organic framework with the addition of urea as a surfactant to form a capacitor electrode material by directly growing MOFs on nickel foam. The 2U-NiCo-MOF exhibited a high specific surface area, which improved its morphological and electrochemical performance. Direct growth without using a binder can overcome the disadvantages of increased contact resistance and reduced energy storage capacity owing to the burying of active sites. In addition, by adding urea, it was possible to improve performance through morphological and electrochemical changes. The large surface area enables the attachment of electrolyte ions; therefore, 2U-NiCo-MOF is an excellent electrode material that can potentially improve the energy density of capacitors. The 2U-NiCo-MOF composite exhibited a high load capacity of 838 F/g at a current density of 2 A/g, while possessing the largest specific capacitance owing to the optimization of the ratios of its constituent components. The optimized 2U-NiCo-MOF composite, therefore, is eminently suitable for application in supercapacitors.

Acknowledgment

This work was supported by a 2-Year Research Grant of Pusan National University.

References

1. J. B, Goodenough, Electrochemical energy storage in a sustainable modern society, *Energy Environ. Sci.*, **7**, 14-18 (2014).
2. M. Shakeel, B. Li, M. Arif, G. Yasin, W. Rehman, A. U. Khan, S. Khan, A. Khan, and J. Ali, Controlled Synthesis of highly proficient and durable hollow hierarchical heterostructured (Ag-AgBr/HHST): A UV and Visible light active photocatalyst in degradation of organic pollutants, *Appl. Catal. B*, **227**, 433-445 (2018).
3. M. Arif, G. Yasin, M. Shakeel, X. Fang, R. Gao, S. Ji, and D. Yan, Coupling of bifunctional CoMn-layered double hydroxide@graphitic C_3N_4 nanohybrids towards efficient photoelectrochemical overall water splitting, *Chem. Asian J.*, **13**, 1045-1052 (2018).
4. D. P. Dubal, O. Ayyad, V. Ruiz, and P. Gomez-Romero, Hybrid energy storage: The merging of battery and supercapacitor chemistries, *Chem. Soc. Rev.*, **44**, 1777-1790 (2015).
5. B. Kang and G. Ceder, Battery materials for ultrafast charging and discharging, *Nature*, **458**, 190-193 (2009).
6. G. Zhou, Graphene–pure sulfur sandwich structure for ultrafast, long-life lithium-sulfur batteries, *Design, Fabrication and Electrochemical Performance of Nanostructured Carbon Based Materials for High-Energy Lithium–Sulfur Batteries*, Springer, Singapore, 75-94 (2017).
7. Y. Zhong, X. Xia, F. Shi, J. Zhan, J. Tu, and H. J. J. Fan, Transition metal carbides and nitrides in energy storage and conversion, *Adv. Sci.*, **3**, 1500286 (2016).
8. D. P. Dubal, N. R. Chodankar and S. Qiao, Tungsten nitride nanodots embedded phosphorous modified carbon fabric as flexible and robust electrode for asymmetric pseudocapacitor, *Small*, **15**,

1804104 (2019).
9. F.-S. Ke, Y.-S. Wu and H. Deng, Metal-organic frameworks for lithium ion batteries and supercapacitors, *J. Solid State Chem.*, **223**, 109-121 (2015).
10. X. Zhang, F. Yang, H. Chen, K. Wang, J. Chen, Y. Wang and S. Song, In Situ Growth of 2D Ultrathin $NiCo_2O_4$ Nanosheet Arrays on Ni Foam for High Performance and Flexible Solid-State Supercapacitors, *Small*, **16**, 2004188 (2020).
11. S. Bi, H. Banda, M. Chen, L. Niu, M. Chen, T. Wu, J. Wang, R. Wang, J. Feng, T. Chen, M. Dinca, A. A. Kornyshev and G. Feng, Molecular understanding of charge storage and charging dynamics in supercapacitors with MOF electrodes and ionic liquid electrolytes, *Nat. Mater.*, **19**, 552-558 (2020).
12. W. Wang, X. Xu, W. Zhou and Z. Shao, Recent progress in metal-organic frameworks for applications in electrocatalytic and photocatalytic water splitting, *Adv. Sci.*, **4,** 1600371 (2017).
13. P. Silva, S. M. F. Vilela, J. P. Tome, and F. A. Almeida Paz, Multifunctional metal–organic frameworks: From academia to industrial applications, *Chem. Soc. Rev.*, **44**, 6774-6803 (2015).
14. L. Shen, Q. Che, H. Li, and X. Zhang, Mesoporous $NiCo_2O_4$ nanowire arrays grown on carbon textiles as binder-free flexible electrodes for energy storage, *Adv. Funct. Mater.*, **24**, 2630-2637 (2014).
15. J. Qi, Y. Yan, Y. Cai, J. Cao, and J. Feng, Nanoarchitectured Design of Vertical-Standing Arrays for Supercapacitors: Progress, Challenges, and Perspectives, *Adv. Funct. Mater.*, **31**, 2006030 (2021).
16. B. Wang, Q. Liu, Z. Qian, X. Zhang, J. Wang, Z. Li, H. Yan, Z. Gao, F. Zhao, and L. Liu, Two steps in situ structure fabrication of Ni–Al layered double hydroxide on Ni foam and its electrochemical performance for supercapacitors, *J. Power Sources*, **246**, 747-753 (2014).
17. C. Wang, J. Xu, M. F. Yuen, J. Zhang, Y. Li, X. Chen, and W. Zhang, Hierarchical composite electrodes of nickel oxide nanoflake 3D graphene for high-performance pseudocapacitors, *Adv. Funct. Mater.*, **24**, 6372-6380 (2014).
18. X. Gong, J. Cheng, F. Liu, L. Zhang, and X. Zhang, Nickel–cobalt hydroxide microspheres electrodepositioned on nickel cobaltite nanowires grown on Ni foam for high-performance pseudocapacitors, *J. Power Sources*, **267**, 610-616 (2014).
19. R. Waghmode, N. Maile, D. Lee, and A. P. Torane, Chemical bath synthesis of $NiCo_2O_4$ nanoflowers with nanorods like thin film for flexible supercapacitor application-effect of urea concentration on structural conversion, *Electrochim. Acta*, **350**, 136413 (2020).
20. T. Y. Wei, C. H. Chen, H. C. Chien, S. Y. Lu, and C. C. Hu, A cost-effective supercapacitor material of ultrahigh specific capacitances: spinel nickel cobaltite aerogels from an epoxide-driven sol–gel process, *Adv. Mater.*, **22**, 347-351 (2010).
21. S. G. Kandalkar, H.-M. Lee, S. H. Seo, K. Lee, and C.-K. Kim, Cobalt–nickel composite films synthesized by chemical bath deposition method as an electrode material for supercapacitors, *J. Mater. Sci.*, **46**, 2977-2981 (2011).
22. C. Qu, L. Zhang, W. Meng, Z. Liang, B. Zhu, D. Dang, S. Dai, B. Zhao, H. Tabassum, S. Gao, H. Zhang, W. Guo, R. Zhao, X. H, M. Liu, and R. Zou, MOF-derived α-NiS nanorods on graphene as an electrode for high-energy-density supercapacitors, *J. Mater. Chem. A*, **6**, 4003-4012 (2018).
23. W. Zhao, Y. Zheng, L. Cui, D. Jia, D. Wei, R. Zheng, C. Barrow, W. Yang, and J. Liu, MOF derived Ni-Co-S nanosheets on electrochemically activated carbon cloth via an etching/ion exchange method for wearable hybrid supercapacitors, *Chem. Eng. J.*, **371**, 461-469 (2019).
24. P. Li, F.-F. Cheng, W.-W. Xiong, and Q. Zhang, New synthetic strategies to prepare metal–organic frameworks, *Inorg. Chem. Front.*, **5**, 2693-2708 (2018).
25. J. Zhao, X. Liu, Y. Wu, D.-S. Li, and Q. Zhang, Surfactants as promising media in the field of metal-organic frameworks, *Coord. Chem. Rev.*, **391**, 30-43 (2019).
26. Y. Tang, Y. Liu, S. Yu, W. Guo, S. Mu, H. Wang, Y. Zhao, L. Hou, Y. Fan, and F. Gao, Template-free hydrothermal synthesis of nickel cobalt hydroxide nanoflowers with high performance for asymmetric supercapacitor, *Electrochim. Acta*, **161**, 279-289 (2015).
27. J. Yang, Z. Ma, W. Gao, and M. Wei, Layered structural co-based MOF with conductive network frames as a new supercapacitor electrode, *Chem. Eur. J.*, **23**, 631-636 (2017).
28. Z.-L. Huang, M. Drillon, N. Masciocchi, A. Sironi, J.-T. Zhao, P. Rabu, and P. Panissod, Ab-initio XRPD crystal structure and giant hysteretic effect (H c= 5.9 T) of a new hybrid terephthalate-based cobalt (II) magnet, *Chem. Mater.*, **12**, 2805-2812 (2000).
29. Y. Liu, Y. He, E. Vargun, T. Plachy, P. Saha, and Q. Cheng, 3D porous Ti3C2 MXene/NiCo-MOF composites for enhanced lithium storage, *Nanomaterials*, **10**, 695 (2020).
30. B. Han, X. Ou, Z. Deng, Y. Song, C. Tian, H. Deng, Y. J. Xu, and Z. Lin, Nickel metal–organic framework monolayers for photoreduction of diluted CO_2: metal-node-dependent activity and selectivity, *Angew. Chem. Int. Ed.*, **57**, 16811-16815 (2018).
31. C. S. Lee, J. Moon, J. T. Park, and J. H. Kim, Engineering, Highly interconnected nanorods and nanosheets based on a hierarchically layered metal–organic framework for a flexible, high-performance energy storage device, *ACS Sustain. Chem. Eng.*, **8**, 3773-3785 (2020).
32. C. S. Lee, J. M. Lim, J. T. Park, and J. H. Kim, Direct growth of highly organized, 2D ultra-thin nano-accordion Ni-MOF@ NiS2@ C core-shell for high performance energy storage device, *Chem. Eng. J.*, **406**, 126810 (2021).
33. J. Xiao and S. Yang, Sequential crystallization of sea urchin-like bimetallic (Ni, Co) carbonate hydroxide and its morphology conserved conversion to porous $NiCo_2$ O_4 spinel for pseudocapacitors, *RSC Adv.*, **1**, 588-595 (2011).
34. H. C. Chen, S. Jiang, B. Xu, C. Huang, Y. Hu, Y. Qin, M. He, and H. J. Cao, Sea-urchin-like nickel–cobalt phosphide/phosphate composites as advanced battery materials for hybrid supercapacitors, *J. Mater. Chem. A*, **7**, 6241-6249 (2019).
35. X. Sun, G. Wang, H. Sun, F. Lu, M. Yu, and J. Lian, Morphology controlled high performance supercapacitor behaviour of the Ni–Co binary hydroxide system, *J. Power Sources*, **238**, 150-156 (2013).
36. A. Eftekhari, The mechanism of ultrafast supercapacitors, *J. Mater. Chem. A* **6**, 2866-2876 (2018).
37. Z. Xiao, Y. Mei, S. Yuan, H. Mei, B. Xu, Y. Bao, L. Fan, W. Kang, F. Dai, R. Wang, L. Wang, S. Hu, D. Sun, and H-C. Zhou, Controlled hydrolysis of metal–organic frameworks: hierarchical Ni/Co-layered double hydroxide microspheres for high-performance supercapacitors, *ACS Nano*, **13**, 7024-7030 (2019).
38. R. B. Waghmode, H. S. Jadhav, K. G. Kanade, and A. P. Torane, Morphology-controlled synthesis of NiCo2O4 nanoflowers on stainless steel substrates as high-performance supercapacitors, *Mater. Sci. Energy Technol.*, **2**, 556-564 (2019).

39. C. Zhang, T. Kuila, N. H. Kim, S. H. Lee, and J. H. Lee, Facile preparation of flower-like $NiCo_2O_4$/three dimensional graphene foam hybrid for high performance supercapacitor electrodes, *Carbon*, **89**, 328-339 (2015).

Authors

Ye Seul Jung; M.Sc., Student, School of Chemical Engineering, Pusan National University, Busan 46241, Korea; jyj980608@ naver.com

Yongju Jung; Ph.D., Full Professor, Department of Applied Chemical Engineering, Korea University of Technology and Education, Cheonan 31253, Korea; yjung@koreatech.ac.kr

Seok Kim; Ph.D., Full Professor, School of Chemical Engineering, Pusan National University, Busan 46241, Korea; seokkim@pusan.ac.kr